ELSEVIER

International Journal of Heat and Fluid Flow 19 (1998) 512–521

International Journal of
HEAT AND
FLUID FLOW

Numerical and modeling influences on large eddy simulations for the flow past a circular cylinder

Michael Breuer [1]

Institute of Fluid Mechanics, University of Erlangen-Nürnberg, Cauerstr. 4, D-91058 Erlangen, Germany

Abstract

In the present work the turbulent flow past a circular cylinder (Re = 3900) was computed by large eddy simulation (LES). The objective was not to investigate the physical phenomena of this flow in detail but to study numerical as well as modeling aspects which influence the quality of LES solutions. Concerning the numerical method the most important component is the discretization of the non-linear convective fluxes. Five different schemes were investigated. Moreover, the influence of different grid resolutions was examined. On the modeling side two aspects play an important role, namely the near-wall model and the subgrid scale (SGS) model. Owing to the restriction to a low Reynolds number in this study, no-slip boundary conditions were used at solid walls. Hence only the second aspect was taken into account. Two different subgrid scale models (Smagorinsky and dynamic model) were applied. Additionally, LES computations without any subgrid scale modeling were carried out in order to prove the performance of the above mentioned SGS models.

Keywords: Large eddy simulation; Modeling error; Discretization error; Accuracy; Bluff Dody flows; Circular cylinder flow

1. Introduction

Turbulent flows past bluff bodies are in general very complicated, including complex phenomena such as separation, reattachment or vortex shedding. An appropriate description by Reynolds-averaged Navier–Stokes equations combined with statistical turbulence models is difficult to achieve. In contrast to statistical turbulence models, direct numerical simulations (DNS) require no extra assumptions but will not be applicable to engineering flows in the near future. The concept of large eddy simulation (LES) offers a suitable way of solving such flow problems. In LES the large eddies depending strongly on the special flow configuration and its boundary conditions are resolved numerically whereas only the fine-scale turbulence has to be modeled by a subgrid scale model.

However, before LES can be used for applications of practical relevance we have to learn more about all influences on the quality of LES solutions. This includes numerical aspects such as discretization schemes or resolution requirements and modeling aspects such as subgrid scale models or near-wall models. Owing to extremely long computation times, detailed studies on this important topic are rare. There have been a few attempts to distribute the load among different groups by organizing workshops on LES for specified test cases. One of these was the "Workshop on LES of Flows Past Bluff Bodies" at Tegernsee, June 1995. The results have been published by Rodi et al. (1997). However, despite the large number of contributions it was quite difficult to draw any concrete conclusions. Different groups applied different numerical methods on grids with varying resolutions using different subgrid scale models and wall boundary conditions. Much of what was learned in terms of how the various factors affect the results was derived from those cases in which a single group made multiple simulations that differed in just one factor.

The objective of the work reported here was to continue such efforts in order to learn more about LES and the important factors affecting the quality of the solution. In contrast to the test cases of the LES workshop at Tegernsee (flow past a square cylinder and flow past a cubical obstacle), which could be tackled by Cartesian grids, a geometrically and physically more complex flow problem is considered, namely the flow past a long, circular cylinder. In contrast to its square counterpart this configuration requires curvilinear body-fitted grids and the separation point on the surface is not fixed by the geometry.

2. Numerical simulation process and accuracy

In Fig. 1 the whole procedure of a numerical simulation is illustrated schematically. The starting point of any simulation is the physical system which should be described. In the context of LES this is, of course, represented by a turbulent flow. First, a mathematical model for the behavior of the physical system has to be defined. This step yields the first of three kinds of systematic errors involved in the simulation procedure. The *modeling error* describes the difference between the behavior of the physical system and the exact solution of the mathematical model. Besides the governing equations, the filter formulation,

[1] E-mail: breuer@lstm.uni-erlangen.de.

0142-727X/98/$ – see front matter
PII: S0142-727X(98)10015-2

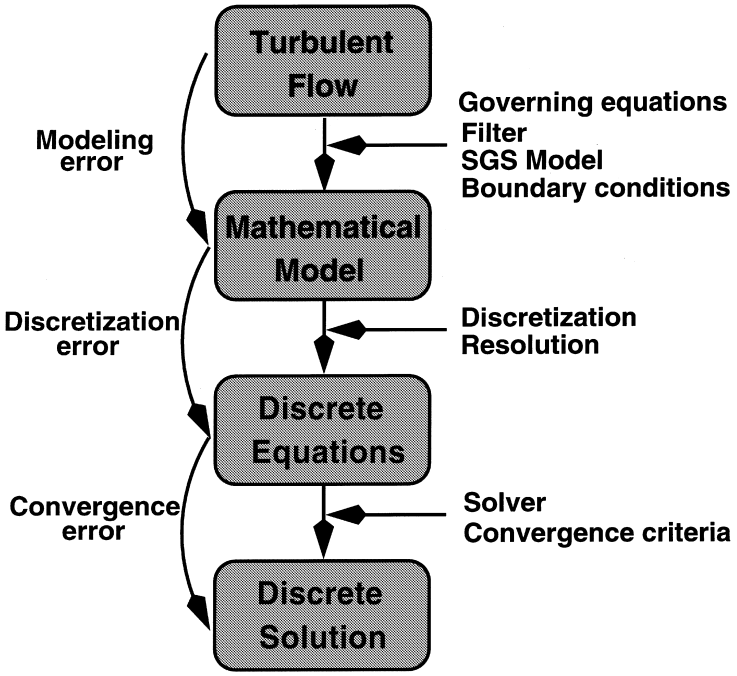

Fig. 1. Numerical and modeling aspects in LES, different kinds of errors involved.

the model for the subgrid scale stresses and the approximations of the boundary conditions determine the size of this type of error in an LES. After selecting a mathematical model, the basic equations have to be discretized because generally no analytical solutions exist for complex physical systems. This introduces the second kind of error, called *discretization error*, defined as the difference between the exact solution of the mathematical model and the exact solution of the discretized equations. In computational fluid dynamics (CFD), the size of this error can be reduced by an appropriate discretization method and a sufficiently fine resolution. Finally, the third type of error, called *convergence error*, arises out of the difference between the iterative and the exact solution of the discretized equations. It depends on the solver applied and the convergence criteria chosen.

These different types of errors should be clearly distinguished even though they are in general totally mixed up in the discrete solution of the physical problem. Nevertheless, one should be aware of these errors strongly influencing the quality of any CFD simulation, not only of LES. In this work we had to restrict the investigations to four aspects, namely the governing equations (2-D versus 3-D), the subgrid scale model, the discretization scheme and the resolution.

3. Description of the LES method

3.1. Finite volume method

For LES the three-dimensional, time-dependent Navier–Stokes equations are filtered in order to separate the large scale and the small scale motions. In this study an incompressible fluid is assumed. A box filter is applied as filter kernel. The governing equations can be found in Breuer and Rodi (1994). The code (LESOCC = Large Eddy Simulation On Curvilinear Coordinates) used to solve the filtered equations is based on a 3-D finite volume method for arbitrary non-orthogonal, body-fitted grids (Breuer and Rodi, 1994, 1996; Breuer et al., 1996a; Breuer et al., 1996b). The surface integrals (F) are approximated by the mid-point rule, which is equivalent to the product of the integrand (f) at the cell face center and the cell face area (S):

$$F_{i+\frac{1}{2}} = \int_{S_{i+\frac{1}{2}}} f \, \mathrm{d}S \approx f_{i+\frac{1}{2}} \cdot S_{i+\frac{1}{2}}.$$

This approximation is of second-order accuracy in space if the value of f is known at the location $i+\frac{1}{2}$. For a cell-centered (non-staggered) grid arrangement as used in LESOCC, the values of f at the cell faces are not available and have to be obtained by interpolation. In order to examine the influence of the interpolation scheme especially for the non-linear convective fluxes, five different options have been investigated. For simplification these schemes are described here under the assumption of an uniform Cartesian grid and a positive flow direction. Then the approximation for the value at the east cell face is as given in Table 1.

The Hybrid scheme is a combination of two different approximations. It toggles between the upwind differencing scheme (UDS) and the central differencing scheme (CDS-2) depending on the local value of the Peclet number Pe. For LES the Peclet number is in general larger than 2. Therefore, the leading truncation error term τ of this scheme is proportional to the grid spacing Δx. The Hybrid scheme satisfies the boundedness criterion unconditionally. However, it is known to be numerically quite diffusive and therefore not well suited for LES. Nevertheless, it is added here for completeness.

The CDS-2 scheme linearly interpolates the value at the cell face which leads to a truncation error term proportional to the square of the grid spacing Δx^2. This error term is dispersive and can manifest itself as $2\,\Delta x$ waves in the solution. In the instantaneous turbulent flow field of LES computations it is extremely difficult to detect such $2\,\Delta x$ waves. However, in most cases these wiggles also occur in the time-averaged flow field. The occurrence of $2\,\Delta x$ waves is an indication of lack of sufficient resolution (see, e.g., Rodi et al., 1997). In general, the probability of wiggles in the solution increases with increasing Reynolds number. For the square cylinder test case at

Table 1
Overview of all interpolation schemes

Scheme	Value at cell face: $f_{i+\frac{1}{2}} =$		τ
Hybrid	$\begin{cases} \frac{1}{2}(f_i + f_{i+1}) \\ f_i \end{cases}$	$\begin{cases} \mathrm{Pe}_{i+\frac{1}{2}} \leqslant 2 \\ \text{otherwise} \end{cases}$	$\begin{cases} \Delta x^2 \\ \Delta x \end{cases}$
CDS-2	$\frac{1}{2}(f_i + f_{i+1})$		Δx^2
HLPA	$f_i + \gamma(f_{i+1} - f_i)\left(\frac{f_i - f_{i-1}}{f_{i+1} - f_{i-1}}\right)$		
	$\gamma = \begin{cases} 1 \\ 0 \end{cases}$	$\begin{cases} 0 < \frac{f_i - f_{i-1}}{f_{i+1} - f_{i-1}} < 1 \\ \text{otherwise} \end{cases}$	$\begin{cases} \Delta x^2 \\ \Delta x \end{cases}$
Quick	$\frac{3}{8}f_{i+1} + \frac{3}{4}f_i - \frac{1}{8}f_{i-1}$		Δx^3
CDS-4	$-\frac{1}{16}f_{i+2} + \frac{9}{16}f_{i+1} + \frac{9}{16}f_i - \frac{1}{16}f_{i-1}$		Δx^4

$\mathrm{Re} = 22{,}000$ Breuer and Pourquié (1996) found 2 Δx waves in front of the cylinder. These originated at the corners of the cylinder and decreased in magnitude when the grid was refined indicating resolution problems in this flow region. For the flow past a circular cylinder at $\mathrm{Re} = 3900$ considered here, no such difficulties were encountered in a large portion of the integration domain. Only in the far field of the cylinder minor wiggles in the solution can be observed (see results below) which, however, are not critical. In general, the CDS-2 scheme has often been used for LES computations.

The HLPA scheme (hybrid linear/parabolic approximation) was proposed by Zhu (1991) and combines a second-order accurate upstream-weighted approximation with first-order accurate upwind differencing under the control of a convection boundedness criterion. Zhu claims that HLPA is capable of yielding low diffusive and always bounded solutions. Especially the first property makes it worth investigating this scheme in the context of LES.

The Quick scheme originally proposed by Leonard (1979) is a logical improvement of the CDS-2 scheme. Instead of a straight line between the nodes i and $i + 1$ a parabola is used to approximate the function f. To construct this polynomial three instead of two nodes have to be taken into account. The third point is taken from the upstream side which is in accordance with the nature of convection. By performing Taylor series expansions it can be shown that this quadratic interpolation has a third-order leading truncation error term. However, it is important to mention that the Quick scheme is still of second-order accuracy if it is used in conjunction with the midpoint rule approximation of the surface integral.

Although this restriction holds true for other higher order interpolations, the CDS-4 scheme was implemented which is the natural extention of CDS-2 and Quick. It fits a third-order polynomial through four nodes. Two nodes are taken from the upstream side and two nodes from the downstream side. Similarly to CDS-2, the CDS-4 scheme is a symmetric interpolation which does not depend on the flow direction like the Hybrid or the Quick scheme. Again, in combination with the mid-point rule this scheme has formally the same order of accuracy as CDS-2, Quick and in most cases HLPA. However, in spite of this fact large differences will be observed in the quality of LES results if these different schemes are used for LES computations. This will demonstrate that the numerical dissipation produced by the scheme for the convective fluxes is of much greater relevance for LES than its formal order of accuracy in space itself. This topic will be discussed below. Finally it should be mentioned that all viscous fluxes are approximated by central differences of second-order accuracy, which fits the elliptic nature of the viscous effects.

Time advancement is performed by a predictor–corrector scheme. A low-storage multi-stage Runge–Kutta method (three substeps, second-order accurate in time) is applied for integrating the momentum equations in the predictor step. Within the corrector step the Poisson equation for the pressure correction (SIMPLE method) is solved implicitly by an incomplete LU decomposition method which is accelerated by a FAS multigrid technique. Explicit time marching works well for LES with small time steps which are necessary to resolve turbulence motion in time. Owing to the higher stability limit of the Runge–Kutta scheme, much larger time steps ($\mathrm{CFL} = \mathrm{O}(1)$) can be used than with the previously applied Adams-Bashforth scheme. This leads to a reduction in computing time by a factor of about 2.

3.2. Subgrid scale models

The filtering procedure provides the governing equations for the resolvable scales of the flow field. They include an additional term for the non-resolvable subgrid scale stresses which describe the influence of the small-scale structures on the larger eddies. For modeling these non-resolvable subgrid scales two different models are applied, namely the well known Smagorinsky model (Smagorinsky, 1963) with Van Driest damping ($l = C_s\,\Delta(1 - \exp(-y^+/25)^3)^{0.5}$) near solid walls as well as the dynamic model originally proposed by Germano et al. (1991). All computations based on the Smagorinsky model have been done with a Smagorinsky constant of $C_s = 0.1$. Following a suggestion by Lilly (1992) a least-squares approach is used to determine values for C_s^2. Depending on the flow problem, different kinds of averaging procedures can be applied in the dynamic approach. For homogeneous flows averaging can be performed in the corresponding direction. For fully inhomogeneous flows only an averaging procedure in time is applicable. Here a recursive low-pass digital filter is chosen (Breuer and Rodi, 1994). In case of the flow past a circular cylinder, it is necessary to average in the homogeneous direction as well as in time (filter parameter $\epsilon = 10^{-3}$) in order to obtain a stable solution. Additionally, negative eddy viscosities are clipped. Moreover, LES computations were performed without any subgrid scale model in order to investigate the influence of the model on the resolved scales. On purpose, these simulations were not called direct numerical simulations because they did not comply with the requirements of DNS. In the author's opinion a simulation should only be denoted as DNS if the spatial and temporal resolution is fine enough to resolve the smallest scales in a turbulent flow, namely the Kolmogorov length and time scale. Regarding to the grids used in the present study (see Table 2), this condition was never fulfilled leading to the notation of "LES without subgrid scale model".

4. Details of the test case

The flow past a long, circular cylinder is an appropriate test case for the intended investigations. First a low (subcritical) Reynolds number of 3900 (based on cylinder diameter D and free-stream velocity u_∞) is chosen. It is known from experiments that for this Reynolds number transition takes place in the free shear layers. The flow problem has already been simulated and analyzed by Beaudan and Moin (1994). For this low

Table 2
Overview of all simulations for the circular cylinder

Run	Grid	Domain	Scheme	SGS Mod.	L_r/D	C_d	$C_{P_{back}}$	Θ_1	Θ_2	Θ_3
A	$165 \times 165 \times 1$	$30D \times \pi D$	CDS-2	–	–	1.625	−2.008	100.7	138.2	–
B1	$165 \times 165 \times 32$	$30D \times \pi D$	Hybrid	Smago.	0.397	1.486	−1.665	95.2	126.0	–
B2	$165 \times 165 \times 32$	$30D \times \pi D$	HLPA	Smago.	0.630	1.319	−1.432	91.4	115.5	–
B3	$165 \times 165 \times 32$	$30D \times \pi D$	Quick	Smago.	1.686	0.969	−0.867	86.7	121.5	150.6
B4	$165 \times 165 \times 32$	$30D \times \pi D$	CDS-2	Smago.	1.115	1.099	−1.049	87.9	112.0	147.3
B5	$165 \times 165 \times 32$	$30D \times \pi D$	CDS-4	Smago.	1.214	1.071	−1.011	87.6	113.7	150.6
C1	$165 \times 165 \times 32$	$30D \times \pi D$	CDS-2	–	0.994	1.144	−1.115	88.6	111.3	150.6
C2 = B4	$165 \times 165 \times 32$	$30D \times \pi D$	CDS-2	Smago.	1.115	1.099	−1.049	87.9	112.0	147.3
C3	$165 \times 165 \times 32$	$30D \times \pi D$	CDS-2	Dynam.	1.197	1.071	−1.011	87.7	113.4	148.8
D1	$165 \times 165 \times 64$	$30D \times \pi D$	CDS-2	–	0.870	1.156	−1.164	89.3	116.7	–
D2	$165 \times 165 \times 64$	$30D \times \pi D$	CDS-2	Smago.	1.043	1.097	−1.069	88.5	119.0	–
D3	$165 \times 165 \times 64$	$30D \times \pi D$	CDS-2	Dynam.	1.372	1.016	−0.941	87.4	–	–
E1	$165 \times 165 \times 64$	$30D \times 2\pi D$	CDS-2	Smago.	1.114	1.089	−1.036	87.9	113.2	146.2
E2	$209 \times 165 \times 32$	$120D \times \pi D$	CDS-2	Smago.	1.106	1.081	−1.023	88.0	112.7	148.9
Experiments (Son and Hanratty, 1969; Norberg, 1987; Cardell, 1993)					1.33 ±0.2	0.98 ±0.05	−0.90 ±0.05	85.0 ±2.0	–	–

Reynolds number simulation no-slip boundary conditions are used at solid walls, whereas for high Reynolds number computations two different wall function approaches are available in LESOCC (Breuer and Rodi, 1994, 1996). In the spanwise direction of the cylinder periodicity of the flow is assumed. At the inflow plane constant velocity is imposed (no perturbations added). A convective boundary condition given by

$$\frac{\partial u_i}{\partial t} + u_\infty \frac{\partial u_i}{\partial x} = 0$$

is used at the outflow boundary. This condition ensures that vortices can approach and pass the outflow boundary without significant disturbances or reflections into the inner domain. In all previous LES computations of different test cases (Breuer and Rodi, 1994, 1996; Breuer and Pourquié, 1996) the convective boundary condition was found to work very well. Likewise, no difficulties were observed in the present case of the circular cylinder flow.

Various curvilinear, O-type grids were generated for this investigation. Table 2 gives an overview of these different grids, the corresponding number of control volumes and the size of the domain. All grids except one consist of 165×165 control volumes in the cross-sectional plane. Primarily two grids were used in this study which only differ in the number of control volumes in the spanwise direction (32 for B/C and 64 for D). The size of the integration domain for these grids is $30D$ in the cross-section and πD in the direction of the cylinder axis. Additionally, three other version are used. The first (Run A) is for a 2-D computation with only one control volume in the spanwise direction. The second (Run E1) is for a test with a larger domain in the spanwise direction, whereas the third (Run E2) covers a four times larger domain in the cross-sectional plane. The internal region of this grid (radius $\leqslant 15D$) is exactly the same as for the other grids. The additional points in the radial direction are added to extend the grid to its new outer size. In all cases the grid points are clustered in the vicinity of the cylinder (geometrical series with a stretching factor of 1.03) and in the wake region.

Statistics were in general compiled over periods of at least $100D/u_\infty$ time units or approximately 22 vortex shedding cycles. In most cases even longer periods of more than $200D/u_\infty$ time units were computed to prove convergence of the statistics. Of course, additional averaging was performed in the spanwise direction.

5. Results and discussion

5.1. Three-dimensional effects

In order to show the necessity for three-dimensional computations for LES, a 2-D simulation was carried out in addition to 3-D simulations. For the 2-D case the same code and the same cross-sectional grid with only one control volume in the spanwise direction were used. Table 2 gives an overview of all simulations. For investigations on the impact of three-dimensionality, simulation A has to be compared with Run C1. Both simulations were carried out with the CDS-2 scheme and no subgrid scale model. Fig. 5 shows the streamlines of the time-averaged flow fields. Totally different streamline patterns can be observed for the 2-D (A) and the 3-D simulations (C1). The largest difference is given by the absence of an attached recirculation region behind the cylinder in the 2-D case.

In spite of nearly the same averaging time for the 2-D and 3-D simulations, the 2-D flow field is more asymmetric than the 3-D flow field. Even increasing the averaging time does not improve the 2-D results significantly. The reason for this strange behavior can only be detected by observations of the instantaneous flow structure past the cylinder. In contrast to the 3-D LES, asymmetric vortex shedding with a non-zero mean lift coefficient is observed in the 2-D case. This phenomenon is shown in Fig. 2 by a plot of the instantaneous pressure distribution. The vortices which shed from the cylinder move downstream along an axis which is inclined with reference to the symmetry line. Irregularly the axis of the vortex street changes from positive to negative angles and the other way round. Similar observations have been reported in the literature. Owing to this behavior, the asymmetric time-averaged streamlines can be explained.

Fig. 3 shows the time-averaged streamwise velocity along the centerline for Run A and Run C1. In contrast with the 3-D

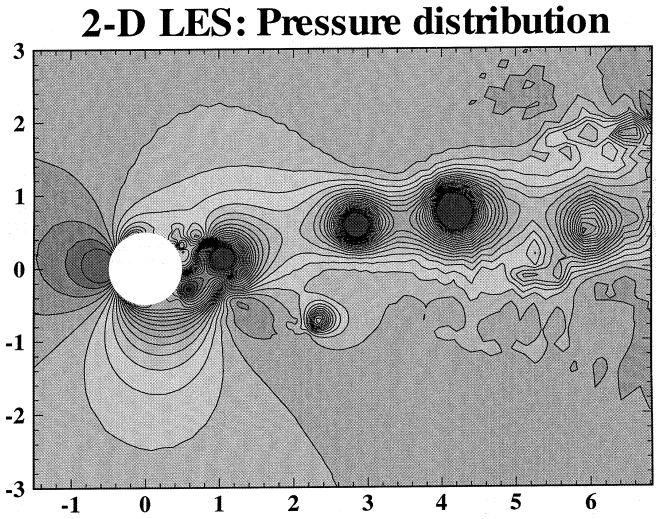

Fig. 2. 2-D LES (Run A): Instantaneous pressure distribution for the flow past a circular cylinder, Re = 3900.

simulation, which predicts a reversed flow region behind the cylinder in accordance with experimental observations by Lourenco and Shih (1993) and Ong and Wallace (1996), the 2-D computation shows no recirculation region at all. Unphyscially, the streamwise velocity is positive along the whole centerline. In the 3-D case (C1) the flow field consists of a large recirculation region behind the cylinder and two additional, small separation bubbles attached to the downstream face of the cylinder (see Fig. 5). As a result of this flow structure the computed drag coefficient C_d and the back-pressure coefficient $C_{P_{back}}$ are much too high in the 2-D case compared with experimental measurements (e.g. Norberg, 1987), Re = 3000: $C_d = 0.98 \pm 0.05$ and $C_{P_{back}} = -0.9 \pm 0.05$). The large deviations between the 2-D and 3-D results indicate that three-dimensional structures strongly influence the near-wake of the flow. Beaudan and Moin (1994) have already pointed out that these structures consist of pairs of counter-rotating streamwise vortices, which cannot be captured by a 2-D calculation. This is an illustrative proof that 2-D LES (as well as DNS) is useless owing to the impact of three-dimensionality of the flow even in case of (nearly) two-dimensional flow problems.

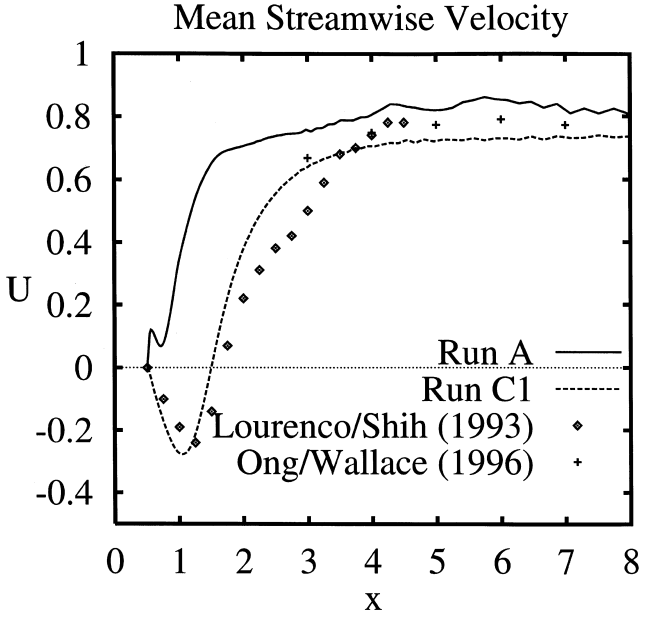

Fig. 3. Mean streamwise velocity along the centerline for Run A (2-D LES) and Run C1 (3-D LES).

Finally, Fig. 4 shows the turbulent von Kàrmàn vortex street past the cylinder visualized by streaklines. Weightless particles released at 20 different sources in the central plane in front of the cylinder were integrated during the flow computation. Of course, the particles do not remain in the central plane. After transition has taken place in the free shear layers of the cylinder they spread in the whole integration domain forming a complex three-dimensional flow structure in the wake.

5.2. Influence of discretization scheme

The second aspect investigated is the influence of different approximations for the convective fluxes in the filtered Navier–Stokes equations. For this purpose five different simulations (Runs B1–B5, see Table 2) were carried out which differed only according to this detail. All simulations were based on the grid with $165 \times 165 \times 32$ control volumes and the Smagorinsky model with $C_s = 0.1$. Fig. 5 shows a first qualitative comparison of the time-averaged streamlines. Although it is already known in the LES community that the discretization scheme plays a dominant role for the quality of the solution, it is worth demonstrating this important issue by illustrative applications. As shown in Fig. 5, the structure and the length of the recirculation bubbles behind the cylinder are strongly influenced by the numerical scheme. In all simulations a recirculation region behind the cylinder exists. Additionally, two small counter-rotating vortices attached to the backward side of the cylinder can be observed. Hence three angles can be determined: the primary separation angle Θ_1, the reattachment angle Θ_2 and the secondary separation angle Θ_3. The values are listed in Table 2 in conjunction with the recirculation length L_r/D, the drag coefficient C_d and the back-pressure coefficient $C_{P_{back}}$. The Strouhal number of the vortex shedding frequency has not been included in Table 2 because for all simulations the computed values are found to be within the experimental range of $St = 0.215 \pm 0.005$ determined by Cardell (1993). Apparently, this quantity is not very sensitive to the parameters of the simulation. Rodi et al. (1997) have already pointed out that accurate prediction of the Strouhal number is not necessarily an indication of a quality simulation.

Fig. 4. Streaklines of the flow past a circular cylinder, Re = 3900.

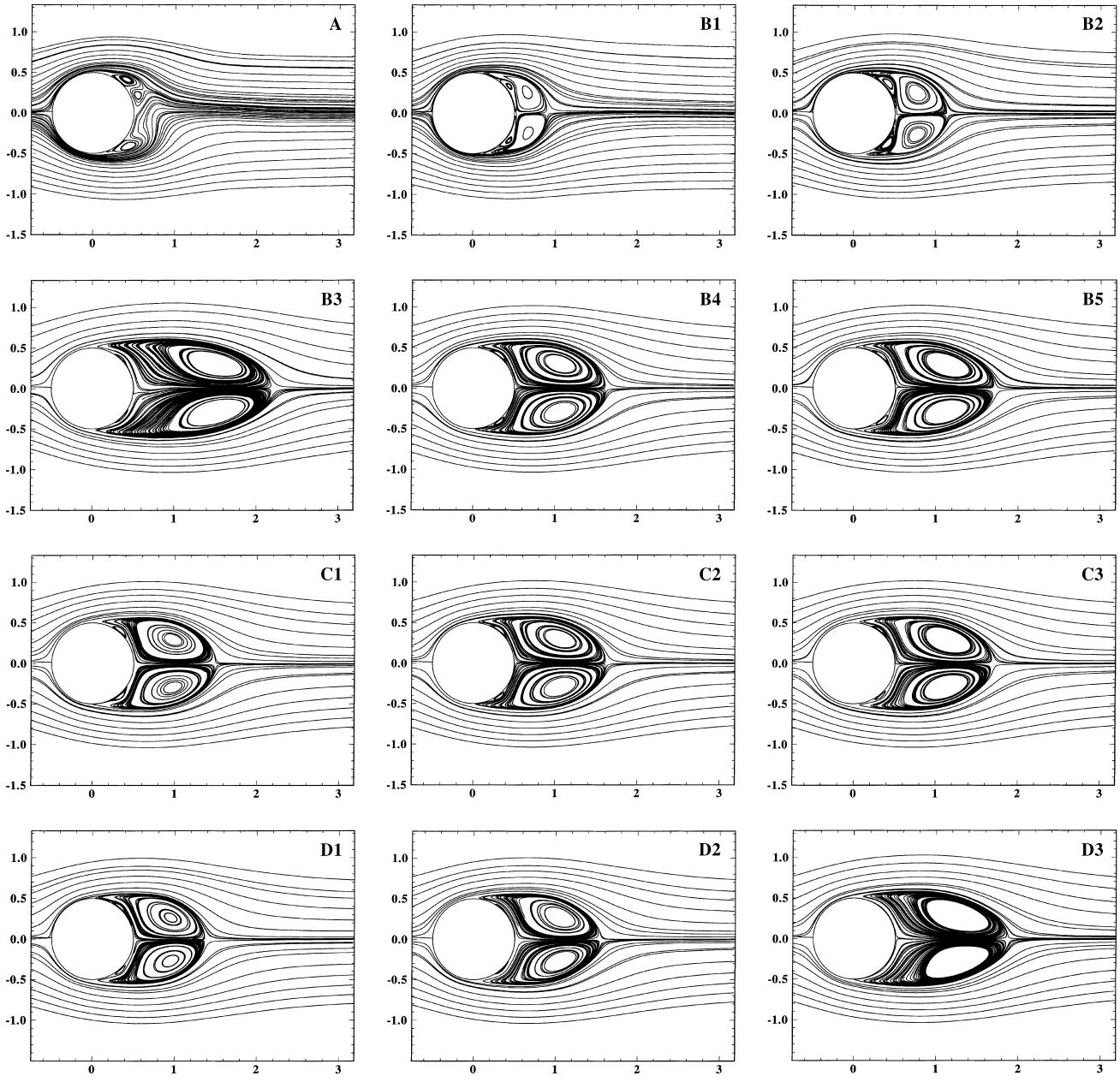

Fig. 5. Time-averaged streamlines for the flow past a circular cylinder, Re = 3900 (for description see Table 2).

As known from measurements (e.g. by Son and Hanratty, 1969), separation should take place before the apex of the cylinder at approximately $\Theta_1 = 85 \pm 2$. In Run B1 (Hybrid scheme) separation is postponed for about 10°. The recirculation length is only one-third of the experimental value resulting in a much too high back-pressure coefficient and drag value. Simulation B2 shows a similar trend. However, the results are quantitatively slightly better but still not in good agreement with the measured values. Run B3, based on the Quick scheme, shows an opposite behavior. Here the computed recirculation length is about 27% larger than the experimental value and the back-pressure and drag coefficients are even smaller than in experiments. This is a totally unexpected result. As already mentioned above, the Quick scheme combined with the mid-point rule is of second-order accuracy. It generates a dispersive third-order error term and also a dissipative fourth-order error term that acts like an additional subgrid scale model. Similarly to the dissipative second-order error term of the Hybrid and the HLPA schemes, the fourth-order term is expected to add numerical diffusion to the problem leading, at least in part, to shorter recirculation zones. However, the Quick scheme shows the opposite result and actually no explanation can be offered for this behavior. Based on experiences with much simpler test cases (e.g. plane channel flow and square duct flow, see, Breuer and Rodi, 1994, 1996) which allow investigations on grids with strongly varying resolutions, no significant improvements of the LES results for the circular cylinder flow are expected for the Quick scheme on finer grids.

The best results compared with experiments (e.g. by Ong and Wallace, 1996) are achieved by the CDS-2 and CDS-4 schemes. The error terms of both schemes do not have any even component (second- or fourth-order derivatives) which damp out high frequency components in the solution. The results of CDS-4 (B5) are in slightly better agreement with experimental observation than those of CDS-2 (B4). However, the variations between these two results are much smaller than among the others.

In Fig. 6 the time-averaged streamwise velocity distribution along the centerline is plotted in comparison with measurements by Lourenco and Shih (1993) and Ong and Wallace (1996). This figure summarizes the observations based on the streamline plots. Additionally, the distribution of the total resolved turbulent kinetic energy k is shown in Fig. 7. The Hybrid scheme (B1) and the HLPA scheme (B2) generate the largest maxima of k close to the cylinder in a distance of about $0.5D$ and $0.75D$, respectively. Additional peaks of k can be observed directly in the vicinity of the wall. The maxima of k produced by CDS-2 (B4) and CDS-4 (B5) are smaller than for B1 and B2 and their locations further downstream. The lowest maximum is achieved by the Quick scheme (B3). In all simulations the position of the maxima coincides fairly well with the recirculation length L_r/D.

However, the high levels of k especially for B1 and B2 have to be explained because they seem to be contradictory to the high numerical diffusion produced by these approximations. In the circular cylinder flow we see strong vortex shedding behind the cylinder accompanied by turbulent fluctuations. Owing to this large-scale vortex shedding the resolved turbulent kinetic energy k is a sum of the quasi-periodic oscillations and the resolved turbulent fluctuations. In order to separate these two effects it would be necessary to perform phase-averaging which is associated with several problems as described by Breuer and Pourquié (1996).

However, looking at instantaneous flow fields of B1–B5 (not shown here) the apparent contradiction turns out fine. In case of B1 and B2 the simulated flow looks like laminar vortex shedding, showing almost no turbulent fluctuations as expected for LES of a turbulent flow. This means that the high levels of k for these simulations are almost completely generated by the quasi-periodic vortex shedding and not by turbulent fluctuations. This observation is consistent with the high level of numerical diffusion typical for upwind schemes (B1 and B2). Simulations B4 and B5 generate instantaneous flow fields as expected for the flow past a cylinder at a subcritical Reynolds number. The vortex shedding motion is superimposed by strong turbulent fluctuations. Again, the result of Run B3 is difficult to explain. Turbulent motions can be observed. However, exact splitting of quasi-periodic and turbulent components cannot be achieved without phase-averaging.

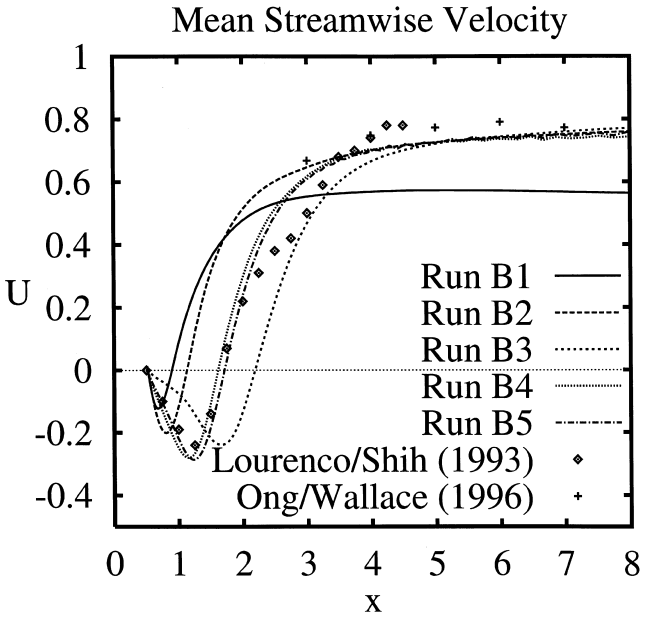

Fig. 6. Mean streamwise velocity along the centerline using different discretization schemes (Runs B1–B5).

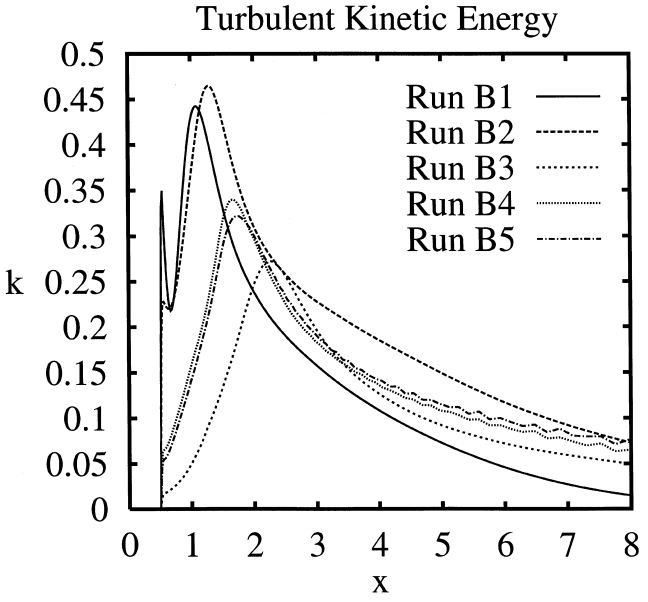

Fig. 7. Total resolved turbulent kinetic energy k along the centerline using different discretization schemes (Runs B1–B5).

5.3. Influence of subgrid scale modeling

In comparison with these large variations of the results applying different numerical schemes, Fig. 5 indicates a small influence of subgrid scale modeling (Runs C1–C3). This is a series of three simulations in which only the model for the non-resolvable subgrid scale stresses was varied. In Table 2 the computed integral quantities are listed. Simulation C1 without any subgrid scale model shows the shortest recirculation length and the highest back-pressure and drag coefficient of all C cases. Applying the Smagorinsky model (C2) results in slightly improved values. The recirculation length increases and accordingly the drag decreases. This trend continues if the dynamic model (C3) is applied instead of the Smagorinsky model. The distribution of the pressure coefficient C_p and the friction coefficient C_f on the surface of the cylinder are plotted in Figs. 8 and 9 for C1–C3. In the front part of the cylinder almost no differences in the results can be observed. Because the flow is laminar in this region, subgrid scale modeling does not have any influence (as expected). However, on the backward side small deviations occur especially for the pressure distribution. The results obtained with the Smagorinsky (C2) and dynamic models (C3) are close to each other and show better agreement with experimental values for a slightly lower Reynolds number of $Re = 3000$ (Norberg, 1987) than C1 without any subgrid scale model. The size of the separation and reattachment regions on the cylinder is similar in all simulations (see Fig. 9).

In Figs. 10 and 11 the time-averaged streamwise velocity and the total resolved turbulent kinetic energy k along the centerline are plotted for Runs C1–C3. As observed before, the location of the maximum of k corresponds fairly well with the recirculation length. It appears that k is reduced when the Smagorinsky model is applied. Surprisingly, k is further reduced when the Smagorinsky model is replaced by the dynamic approach.

5.4. Influence of resolution

In order to investigate the influence of the spanwise resolution, a new series of simulations D1–D3 has been carried out which differs from C1–C3 only by the doubled number of control volumes. Again, Fig. 5 shows the streamline plots of the time-averaged flow and Table 2 lists the computed integral parameters. The largest deviation between a D and a corresponding C result occurs for the simulation applying the dynamic model (C3/D3). In Fig. 12 the turbulent kinetic energy k along the centerline is plotted. Fig. 13 shows the pressure distribution on the surface of the cylinder. In comparison with the results of series C in Fig. 11, k increases for all subgrid scale models and the deviations between the results achieved with different models do not decrease on improving the spanwise resolution. For the pressure distribution the deviations are even emphasized. However, Run D3 shows a fairly good agreement with the measurements of Norberg (1987) ($Re = 3000$) as well as with the integral quantities listed in Table 2.

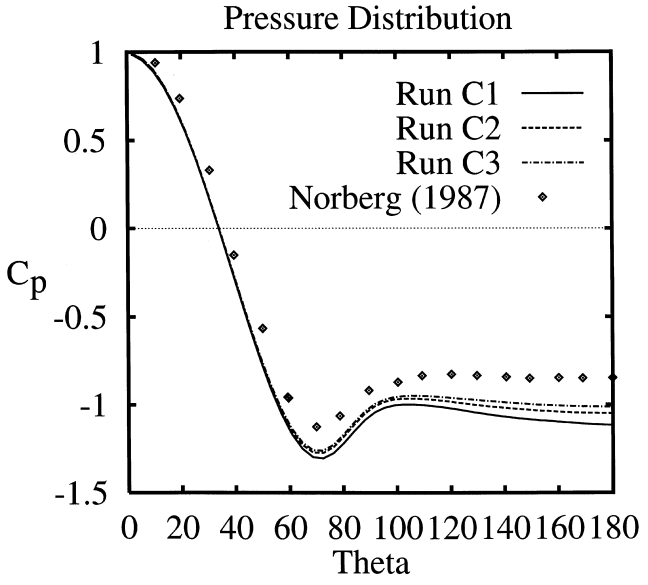

Fig. 8. Pressure coefficient C_p on the surface of the cylinder using different subgrid scale models (Runs C1–C3).

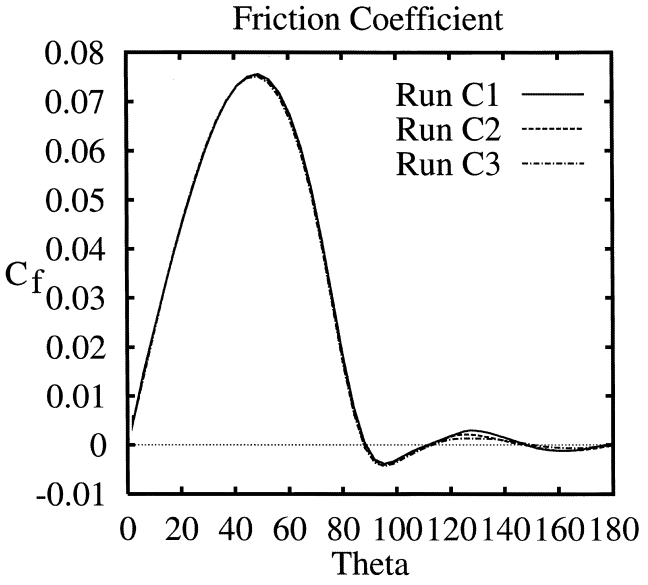

Fig. 9. Friction coefficient C_f on the surface of the cylinder using different subgrid scale models (Runs C1–C3).

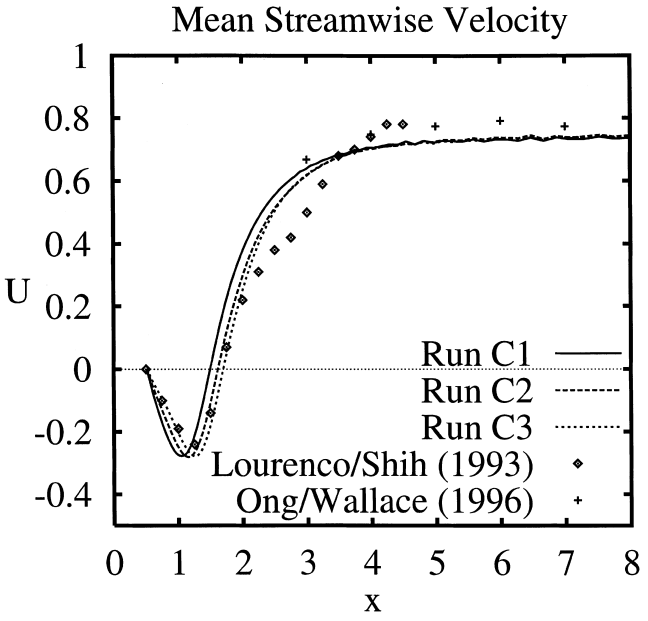

Fig. 10. Mean streamwise velocity along the centerline using different subgrid scale models (Runs C1–C3).

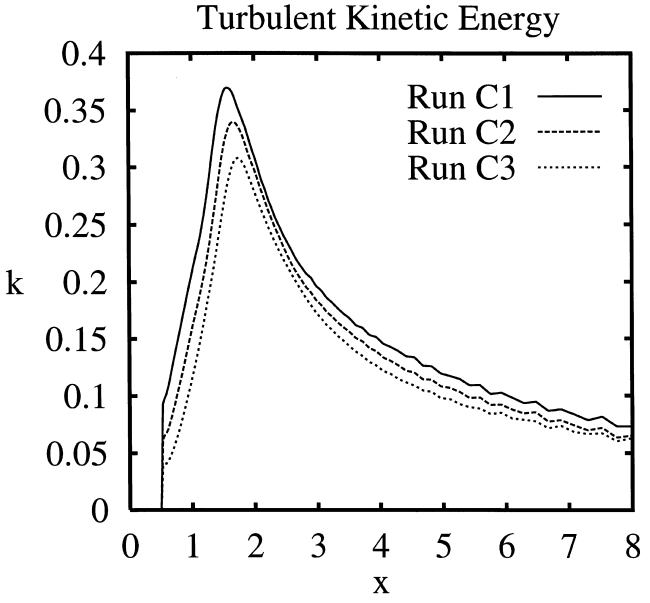

Fig. 11. Total resolved turbulent kinetic energy k along the centerline using different subgrid scale models (Runs C1–C3).

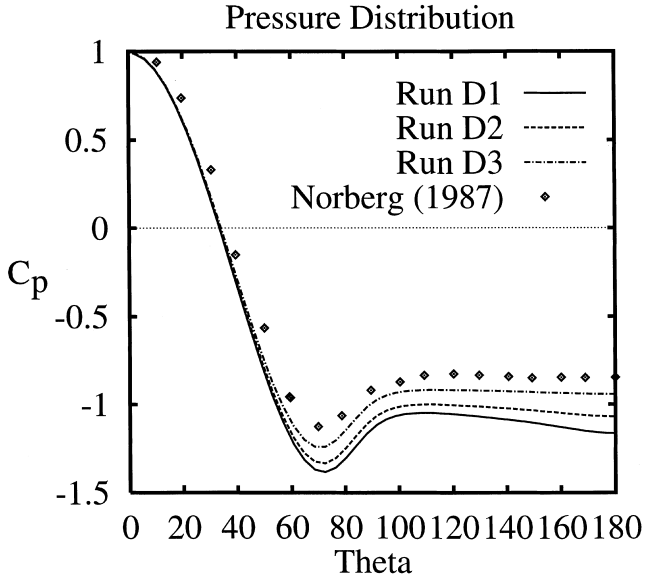

Fig. 13. Pressure coefficient C_p on the surface of the cylinder for Runs D1–D3.

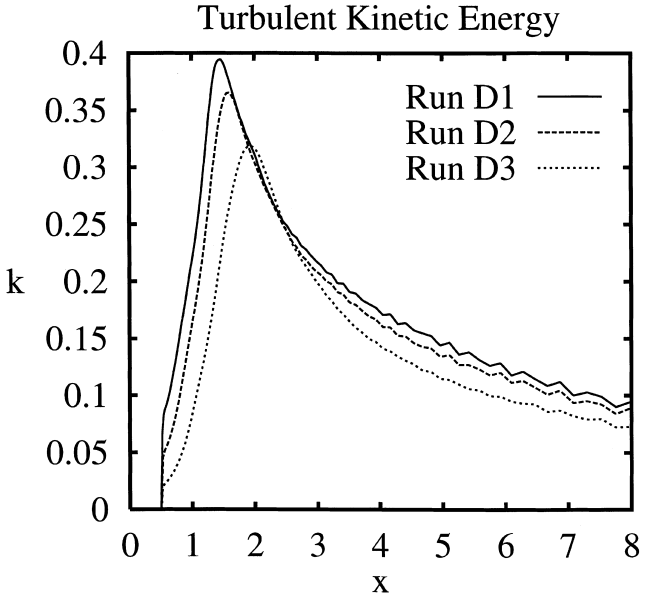

Fig. 12. Total resolved turbulent kinetic energy k along the centerline for Runs D1–D3.

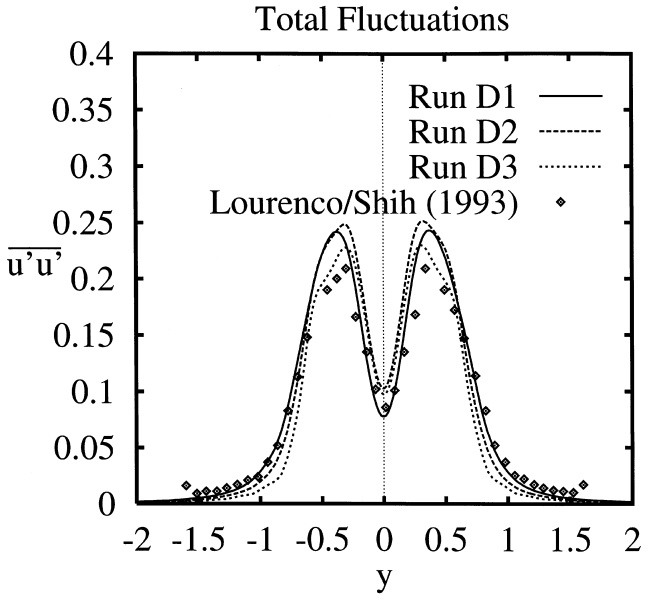

Fig. 14. Total resolved Reynolds stress $\overline{u'u'}$ at $x/D = 1.54$ for Runs D1–D3.

Figs. 14 and 15 show total resolved Reynolds stress profiles in the near wake ($x/D = 1.54$) obtained from D1–D3. For all simulations the streamwise Reynolds stress $\overline{u'u'}$ is fairly well predicted in comparison with measurements by Lourenco and Shih (1993). The dynamic model (D3) yields slightly better results. However, the cross-stream Reynolds stress $\overline{v'v'}$ is highly overpredicted in the simulation without any subgrid scale model (D1) and with the Smagorinsky model (D2). This result is totally contradictory to the observations by Beaudan and Moin (1994), who found underpredicted values of this quantity. Again, the dynamic model (D3) shows an excellent agreement with the measurements according to the simulations by Beaudan and Moin (1994). The differences between the present results and those by Beaudan and Moin (1994) are expected to be almost entirely due to numerical effects. On the one hand a different grid point distribution and grid stretching may be responsible for these deviations. On the other hand, however, the impact of the numerical dissipation produced by the higher-order upwind-biased schemes (fifth- and seventh-order) applied in the simulations by Beaudan and Moin (1994) should definitely play a more dominant role as it was already demonstrated for other upwind schemes above.

Finally, two more aspects were investigated. First the domain of integration is doubled in the spanwise direction (Run E1) by doubling the number of grid points compared with C2 while keeping the spanwise cell size constant. According to the computed integral parameters, this modification does not improve the results significantly. Another test (Run E2) increases

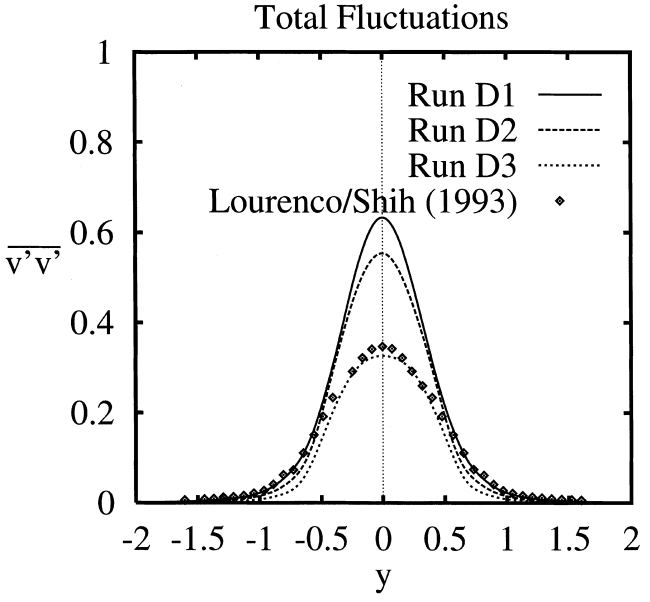

Fig. 15. Total resolved Reynolds stress $\overline{v'v'}$ at $x/D = 1.54$ for Runs D1–D3.

the domain of integration four times in the radial direction while keeping the internal grid unchanged (as described above). Also this modification is rather irrelevant to the computed results, indicating that the previously used domain size is fully sufficient.

6. Conclusions

The flow past a circular cylinder at a subcritical Reynolds number of $Re = 3900$ was simulated by the method of LES. The objective of the present work was not to study the physics of this flow in detail but to carry out an extensive investigation on numerical and modeling aspects influencing the quality of LES solutions. The strong impact of three-dimensionality for LES calculations as well as the important aspect of low-diffusive discretization schemes for the convective fluxes were presented and discussed. The investigation confirmed the statement that the numerical dissipation produced by a scheme is more crucial for LES than its formal order of accuracy. Furthermore, the influence of subgrid scale modeling and spanwise resolution was studied in detail. Drawing conclusions from the investigations above, the dynamic model (D3) yields the best solution which agrees fairly well with experimental measurements. Finally, the important role of the spanwise resolution, which has often been underestimated for LES (and DNS) of flow problems with a homogeneous direction, must be emphasized.

Acknowledgements

Financial support by the Bayerische Forschungsstiftung in the Bavarian Consortium of High-Performance Scientific Computing (FORTWIHR II) is gratefully acknowledged.

References

Beaudan, P., Moin, P., 1994. Numerical experiments on the flow past a circular cylinder at a subcritical Reynolds number, Report No. TF-62, Thermosciences Division, Department of Mechanical Engineering, Stanford University.

Breuer, M., Pourquié, M., 1996. First experiences with LES of flows past bluff bodies. In: Rodi, W., Bergeles, G. (Eds.). Proc. of the 3rd Intern. Symp. of Engineering Turbulence Modelling and Measurements, Herakilon, Crete, Greece, 27–29 May 1996, Engineering Turbulence Modelling and Exp., vol. 3, Elsevier, Amsterdam, pp. 177–186.

Breuer, M., Pourquié, M., Rodi, W., 1996a. Large-eddy simulation of internal and external flows. In: Kreuzer, E., Mahrenholtz, O. (Eds.), 3rd Int. Congress on Indust. and Applied Mathem., Hamburg, 3–7 July 1995, Special Issue of ZAMM, Issue 4: Applied Sciences – Especially Mechanics (Minisymp.), Akademie Verlag, Berlin, pp. 235–238.

Breuer, M., Lakehal, D., Rodi, W., 1996b. Flow around a surface mounted cubical obstacle: comparison of LES and RANS-results. In: Deville, M., Gavrilakis, S., Rhyming, I.L. (Eds.), IMACS-COST Conf. on CFD, 3-D Complex Flows, Lausanne, Switzerland, 13–15 September 1995, Comp. of 3-D Complex Flows, Notes on Numerical Fluid Mech., vol. 53, Vieweg Verlag, Braunschweig, pp. 22–30.

Breuer, M., Rodi, W., 1994. Large-eddy simulation of turbulent flow through a straight square duct and a 180° bend. Fluid Mech. and its Appl., vol. 26, Direct and Large-Eddy Simulation I, In: Voke, P.R., Kleiser, L., Chollet, J.P. (Eds.), Selected Papers from the first ERCOFTAC Workshop on DNS and LES, Guildford, Surrey, UK, 27–30 March 1994, Kluwer Academic Publishers, Dordrecht, pp. 273–285.

Breuer, M., Rodi, W., 1996. Large-eddy simulation of complex turbulent flows of practical interest. In: Hirschel, E.H. (Ed.), Flow Simulation with High-Performance Computers II, Notes on Numerical Fluid Mechanics, vol. 52, Vieweg Verlag, Braunschweig, pp. 258–274.

Cardell, G.S., 1993. Flow Past a Circular Cylinder with a Permeable Splitter Plate, Ph.D. Thesis, Graduate Aeronautical Lab., California Inst. of Technology.

Germano, M., Piomelli, U., Moin, P., Cabot, W.H., 1991. A dynamic subgrid scale eddy viscosity model. Phys. Fluids A 3 (7), 1760–1765.

Leonard, B.P., 1979. A stable and accurate convection modelling procedure based on quadratic upstream interpolation. Comput. Methods Appl. Mech. Eng. 19, 59–98.

Lilly, D.K., 1992. A proposed modification of the Germano subgrid-scale closure method. Phys. Fluids A 4 (3), 633–635.

Lourenco, L.M., Shih, C., 1993. Characteristics of the plane turbulent near wake of a circular cylinder, a particle image velocimetry study, private communication (data taken from Beaudan and Moin, 1994).

Norberg, C., 1987. Effects of Reynolds Number and Low-Intensity Free-Stream Turbulence on the Flow around a Circular cylinder, Publ. No. 87/2, Department of Applied Thermosc. and Fluid Mech., Chalmer University of Technology, Gothenburg, Sweden.

Ong, L., Wallace, J., 1996. The velocity field of the turbulent very near wake of a circular cylinder, Exp. in Fluids, vol. 20, Springer Verlag, Berlin, pp. 441–453.

Rodi, W., Ferziger, J.H., Breuer, M., Pourquié, M., 1997. Status of Large Eddy Simulation: Results of a Workshop, Workshop on LES of Flows Past Bluff Bodies, Rottach-Egern, Tegernsee, Germany, 26–28 June 1995; J. Fluids Eng. 119 (2), 248–262.

Smagorinsky, J., 1963. General circulation experiments with the primitive equations I, the basic experiment. Mon. Weather Rev. 91, 99–165.

Son, J., Hanratty, T.J., 1969. Velocity gradients at the wall for flow around a cylinder at Reynolds numbers from 5×10^3 to 10^5. J. Fluid Mech. 35, 353–368.

Zhu, J., 1991. A low-diffusive and oscillation-free convection scheme. Commun. Appl. Num. Meth. 7, 225–232.